Journal of Materials Chemistry A

ROYAL SOCIETY OF CHEMISTRY

PAPER

View Article Online
View Journal | View Issue

Cite this: J. Mater. Chem. A, 2025, 13, 27279

Controlling metal–organic framework crystallization *via* computer vision and robotic handling†

Kai Xiang Chong, ‡[a] Qusai Abdulkhaliq Alsabia,‡[b] Zuyang Ye,[a] Andrew McDaniel,[a] Douglas Baumgardner,[b] Dianne Xiao *[b] and Shijing Sun*[a]

Traditional experimental techniques for metal–organic frameworks (MOFs) crystal growth are often time-consuming due to the need for manual bench chemistry and data analysis. In this study, we integrated laboratory automation with computer vision to accelerate the synthesis and characterization of Co-MOF-74, a porous framework containing coordinatively unsaturated Co(II) sites. By utilizing a liquid-handling robot, we significantly improved the efficiency of precursor formulation for solvothermal synthesis, saving approximately one hour of manual hands-on labor per synthesis cycle. We developed an accelerated characterization strategy using high-throughput optical microscopy and computer vision to identify the quality of crystallization outcomes. Our computer vision framework, Bok Choy Framework, enabled automated feature extraction from microscopic images, improving the analysis efficiency by approximately 35 times compared to manual analysis methods. Using this integrated workflow, we systematically performed a rapid screening of synthesis parameters and examined how each parameter influenced the crystal morphology. Furthermore, by varying solvent compositions, we rapidly screened synthesis conditions that modulated crystal formation, identifying regimes that promoted crystallization or inhibit growth. The resulting structured dataset linking synthesis conditions to crystal morphology provided a scalable foundation for data-driven materials discovery. The combination of automated experimentation and data analysis establishes a cost-effective and widely applicable platform for accelerating research of functional materials, with broad applications in catalysis, energy storage, and beyond.

Received 23rd April 2025
Accepted 15th July 2025

DOI: 10.1039/d5ta03199k

rsc.li/materials-a

[a]Department of Mechanical Engineering, University of Washington, Seattle, Washington 98195, USA. E-mail: shijing@uw.edu
[b]Department of Chemistry, University of Washington, Seattle, Washington 98195, USA. E-mail: djxiao@uw.edu

† Electronic supplementary information (ESI) available. See DOI: https://doi.org/10.1039/d5ta03199k

‡ These authors contributed equally to this work.

Shijing Sun

Dr Shijing Sun is an assistant professor at the University of Washington, leading the UW Sun Lab. Her research focuses on collaborative intelligence, augmenting human expertise, robotics, and artificial intelligence to accelerate development of energy materials. Before joining University of Washington, Dr Sun was a senior research scientist at the Toyota Research Institute, where she researched AI-powered solutions for accelerated materials discovery and design for electric vehicle batteries and fuel cells. She was a research scientist at MIT, leading the Accelerated Materials Team on development of machine learning-guided high-throughput experimentation for photovoltaics. Dr Sun completed her academic studies at Trinity College, University of Cambridge, where she earned her BA in Natural Sciences, and MS and PhD in Materials Science.

1 Introduction

In recent years, metal–organic frameworks (MOF) have gained significant attention due to their high surface area, tunable porosity, and diverse chemical functionality, enabling applications in gas storage, catalysis, and separation technologies.[1] These crystalline materials, composed of metal-containing nodes and organic linkers, exhibit ultrahigh porosity and adjustable surface properties.[2–4] However, optimizing MOF synthesis remains a key challenge due to the difficulty of consistently controlling crystal phase, shape, and size across varying reaction conditions.[5] This inconsistency stems from the large and interdependent synthetic parameter space, where variations in parameters such as solvent composition, temperature, reaction time, and precursor concentration can result in diverse morphologies or failure to crystallize altogether. Moreover, MOF formation is highly sensitive to minor fluctuations in synthesis conditions, making manual optimization difficult and often irreproducible.[6] A systematic approach is required to efficiently explore synthesis conditions and establish reproducible pathways for controlling MOF formation. To address this challenge, high-throughput experimentation using robotic platforms has emerged in the field of MOFs to reduce experimental time and improve reproducibility.[7,8] Since crystal size and morphology influence key properties such as gas adsorption capacity and diffusion pathway, precise control over both MOF crystal size and aspect ratios (ARs) is desirable.[5]

Among various MOFs, this study focuses on Co_2(dobdc) (dobdc^{4-} = 2,5-dioxido-1,4-benzenedicarboxylate), a member of the M_2(dobdc) or MOF-74 series, where M represents divalent transition metal ions such as Mg^{2+}, Mn^{2+}, Fe^{2+}, Co^{2+}, Ni^{2+}, and Zn^{2+}. The MOF-74 series was first reported for Zn-based frameworks by Yaghi *et al.*, while the cobalt-based variant was later reported by Dietzel *et al.*[9,10] These MOFs feature Lewis acidic metal centers and Lewis basic organic linkers, forming a robust and versatile structure for various applications, such as hydrogen storage, gas adsorption, and separation.[11,12] Co_2(dobdc) is particularly valuable due to its high stability, strong metal–ligand interactions, and high porosity, making it an excellent candidate for carbon dioxide absorption and hydrocarbon separation.[13]

Accurate characterization of MOF crystals is equally critical but remains slow and resource-intensive. Scanning electron microscopy (SEM) enables high-resolution imaging for analyzing crystal size and morphology, but requires extensive sample preparation, vacuum environments, and prolonged imaging times, making it low-throughput and costly.[14] In contrast, optical microscopy (OM) offers a rapid and cost-effective alternative for initial morphology assessment, but manual image analysis is time-consuming and subjective.[15] To overcome these limitations, computer vision algorithms have emerged as powerful tools to automate feature extraction. For instance, computer vision has been used for defect detection and tracking the dynamic behavior of MOFs in electron microscopy images.[16,17] By enhancing characterization techniques, computer vision provides an efficient and scalable solution for high-throughput morphology analysis, significantly reducing the need for human intervention.

In this study, we developed an integrated workflow that combines automated MOF synthesis with high-throughput optical microscopy and computer vision-assisted image analysis for rapid morphological screening. Utilizing the Opentrons OT-2 liquid handling robot, we systematically explored synthesis conditions for Co_2(dobdc), ensuring precise and reproducible sample preparation. To streamline characterization, we developed a computer vision algorithm, named Bok Choy Framework, that automated image processing, enabling rapid and accurate identification of isolated crystals and clusters in microscopic images and extracting key morphological features. These extracted values were subsequently used for high-efficiency and high-accuracy data analysis. Unlike previous robotic workflows that primarily focused on sample preparations and SEM-based phase identification, our approach directly maps synthesis parameters to crystal morphology at a single-crystal level. Leveraging this workflow, we systematically screened reaction time, temperature, precursor concentrations, and solvent composition, identifying critical factors that influence crystallization and morphological variations. We further demonstrated how high-throughput approaches can accelerate MOF synthetic optimization through the construction of a scalable, structured dataset that links synthesis conditions to synthetic outcome and crystal morphology. By integrating automation with data-driven analysis, our workflow bridged traditional synthesis and high-throughput materials screening, enabling precise, efficient, and scalable control over MOF crystallization.

2 Results and discussion

2.1 Overview of data collection and analysis workflow

Fig. 1 illustrates the schematic of the robot and computer vision-assisted experimental workflow for MOF crystallization. The workflow consists of three stages: high-throughput synthesis, high-throughput characterization, and computer-vision-enhanced image analysis. In the synthesis stage, samples were prepared using a liquid handling robot (named Mara) to automate the pipetting and dispensing of MOF precursor solutions, ensuring consistency and reproducibility. Using a 300 μL pipette as a reference, Mara was able to aspirate 300 μL and dispense the solutions into three wells, refill, and repeat across a 96-well plate in 8 minutes and 18 seconds, achieving a mass error of only 0.105% (see ESI Section S2† for more details). The as-synthesized samples were subsequently analyzed in the characterization stage using high-resolution optical microscopy (EVOS imaging system with automated XY stage), allowing high-throughput imaging without manual repositioning. This setup significantly improved imaging throughput and consistency across multiple samples. In the image analysis stage, we developed the Bok Choy Vision Framework to detect and classify crystalization outcomes. Quantitative features, including the aspect ratio of single crystals and the crystal area, were extracted and analyzed. These

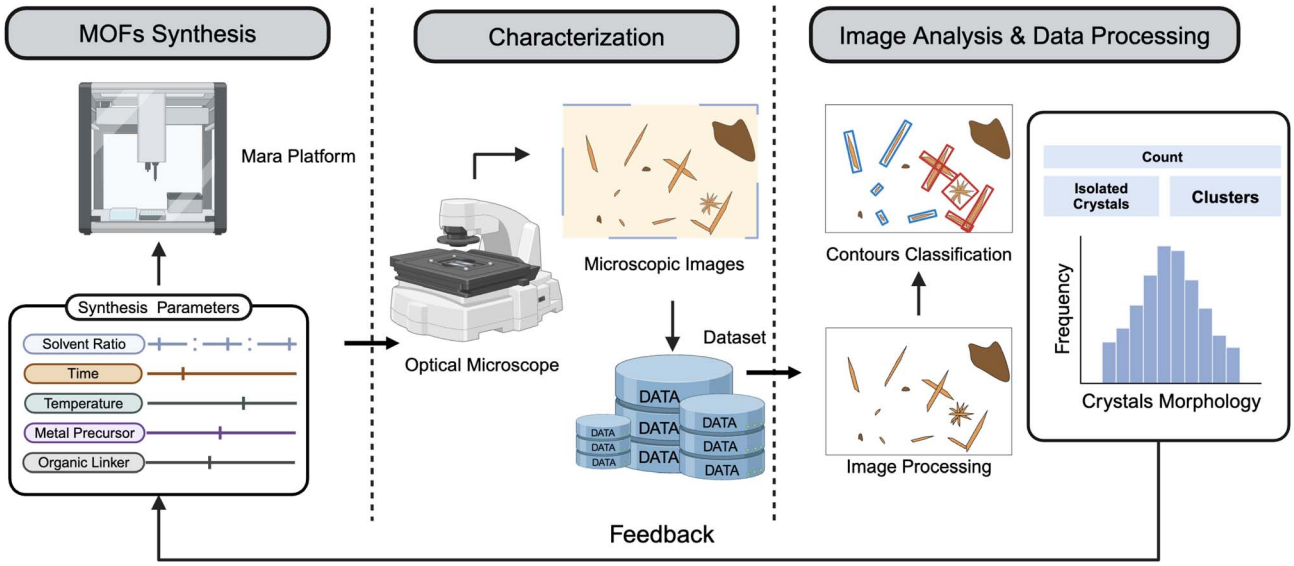

Fig. 1 Schematic illustration of the closed-loop workflow of the synthesis and optimization of MOF materials. Initial synthesis parameters were programmed into the OT-2 liquid handling robot, which automated the dispensing of MOF precursors. The synthesized samples were then characterized using an optical microscope to capture their brightfield images. These images were processed using computer vision techniques for morphological classification, and the extracted features were subsequently analyzed to guide the selection of the next set of synthesis parameters.

insights enabled a faster, more efficient feedback loop between synthesis and characterization.

2.2 High-throughput synthesis and characterization

Controlling solvent composition and ratio, reaction time, temperature, and precursor stoichiometry is critical for modulating the nucleation and growth of MOF crystals. However, previous studies have focused predominantly on one or a few variables at a time due to the complexity of the high-dimensional synthesis space.[5,18,19] In this work, a high-throughput synthesis platform was implemented to explore a five-dimensional parameter space, allowing systematic and data-driven control over the crystal morphology of MOFs. The automated sample preparation setup for synthesizing Co_2(dobdc) using Mara is illustrated in Fig. 2a. We first randomly selected six solvent conditions while keeping other synthesis parameters (*e.g.*, reaction time, temperature) constant (see ESI Table S1† for experimental details) with the goal of training the robot to follow synthetic protocols of MOF crystallization. We programmed the liquid handling robot to automatically perform precursor formulation tasks using three solvent systems: dimethylformamide (DMF), water, and ethanol. Compared to manual synthesis, although the robotic platform completed the formulation of a single precursor solution in

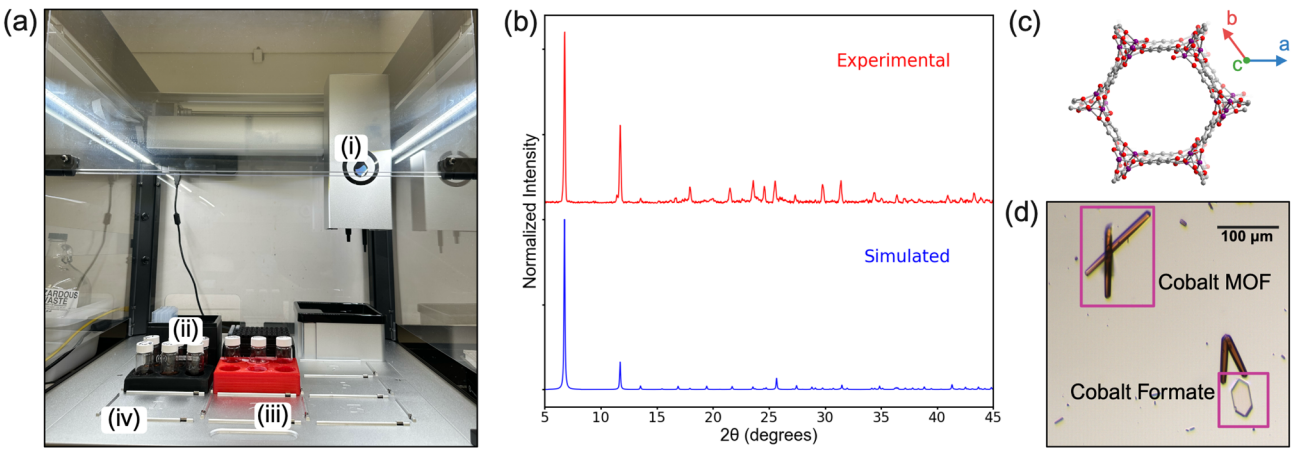

Fig. 2 (a) Photograph of the automated synthesis system using an Opentrons OT-2 liquid handling robot. Insets show the (i) Opentrons pipette, (ii) pipette tips, (iii) precursor solvents, and (iv) final products. (b) X-ray diffraction (XRD) pattern of synthesized Co_2(dobdc) compared with the simulated reference pattern from the Cambridge Crystallographic Data (c) The crystal structure of Co_2(dobdc). Purple, red, gray, blue, and white spheres represent Co, O, C, N, and H atoms, respectively. (d) Microscopic images of the synthesized Co_2(dobdc) crystals, showing the desirable MOF alongside a common side product (cobalt formate).

a similar amount of time, it ensured precise reagent handling, minimized human error, and significantly reduced hands-on labor by approximately one hour per synthesis cycle through automated pipetting. This reduction in manual time, along with improved precision, enhanced experimental consistency, and accelerated synthesis throughput, facilitating the development and optimization of MOF materials (see ESI Section S2† for benchmarking details).

Structural characterization using X-ray diffraction (XRD) confirmed the successful formation of Co_2(dobdc), as shown in Fig. 2b, following solvothermal synthesis using Mara. While XRD is the gold standard for phase identification, inline proxy measurements are attractive for their lower cost and faster feedback before full structural characterization. Optical microscopy, particularly when integrated with an automated scanning stage, enables high-throughput characterization with acquisition times on the order of seconds, making it a powerful tool for the rapid screening of large numbers of MOF crystals. In this study, XRD was used to confirm the formation of Co_2(dobdc), and optical microscopy (OM) served as a high-throughput proxy to assess crystallization outcomes. Initially, rod-shaped crystals observed *via* OM were cross-validated with XRD to confirm their identity as Co-MOF-74. This characteristic morphology was then used as a system-specific indicator of successful MOF formation. Additionally, OM facilitated binary classification of crystallization outcomes (crystals *vs.* no crystals), enabling efficient early-stage screening across large experimental spaces. The Co_2(dobdc) crystals exhibit anisotropic growth along the *c*-axis, forming one-dimensional chains through coordination of dobdc ligands with the Co^{2+} centers, resulting in hexagonal channels as shown in Fig. 2c.[5] This morphology is readily distinguishable from that of cobalt formate, which typically crystallizes as hexagonal, plate-like pink crystals. A representative optical image of as-synthesized Co_2(dobdc) is shown in Fig. 2d, highlighting well-defined rod-like MOF crystals, along with a commonly observed side product, cobalt formate. Furthermore, key morphological features such as aspect ratio and cross-sectional area were identified as important parameters to quantify the anisotropic crystal growth. In addition to rapid identification of target and side products, optical microscopy provides immediate access to information on crystal size and morphology, which are more challenging to extract from bulk XRD alone. The use of microscopy, in combination with computer vision-based image analysis, presents a low-cost, high-throughput alternative for the preliminary examination of crystallization outcomes for inorganic synthesis. This approach holds broad potential for enabling autonomous experimental workflows in chemical and materials laboratories, beyond the scope of MOF synthesis demonstrated in this work.

2.3 Synthetic screening for MOF-74 crystalization

The aspect ratio results from the initial six synthesis conditions were successfully analyzed using the Bok Choy algorithm, as shown in Fig. S1.† The aspect ratios were visualized in a heat map (Fig. S2†) to illustrate variations across different solvent concentrations. Crystals with shorter dimensions along the *c*-axis are expected to enhance gas absorption efficiency due to a reduced diffusion path.[5] Among the initial six conditions, the SolventVolumes-3I condition yielded the lowest aspect ratio (1.40). Hence, this condition was selected as the benchmark for further optimization to systematically investigate the impact of reaction time, temperature, amount of metal precursors, and amount of organic linkers on the growth of MOF crystal.

To determine the optimal conditions, a synthetic screening approach was adopted. Representative images from each condition were selected based on image quality for subsequent morphological analysis (see ESI Table S3† for morphological data). Taking advantage of the robot-assisted synthesis and high-throughput characterization, rapid screening of the synthesis parameters was conducted. As shown in Fig. 3a and b, reaction time and temperature play critical roles in determining the size and the morphology of Co_2(dobdc). Under a tri-solvent system with a fixed solvent ratio of water : DMF : ethanol = 2 : 1 : 2, crystallization was not observed at short reaction time (<21 h) or low temperatures (<90 °C), indicating that insufficient energy input and reaction duration are required for nucleation and crystal growth.[20] At 24 hours and 100 °C, well-defined crystals were obtained, whereas prolonged reaction times or elevated temperatures led to elongated morphologies, irregular shapes, or aggregation, consistent with the literature results.[18] Additionally, the stoichiometric balance between metal precursors and organic linkers also affected nucleation and crystal growth, as shown in Fig. 3c and d. Insufficient or excessive precursors hindered metal–ligand complexation, preventing the formation of well-defined crystal structures. Low linker concentrations produced scant, small, and elongated crystals, while high linker concentrations resulted in the formation of nucleation clusters, leading to excessive side products. This screening approach demonstrates the effectiveness of automated synthesis and high-throughput characterization in rapidly identifying suitable conditions for MOF crystallization and systematically mapping the effects of synthesis parameters on nucleation and crystal growth.

2.4 Computer vision-assisted crystallization outcome quantification

Traditionally, scientists manually extract crystal size and morphology from microscopic images. However, with robotic synthesis and high-throughput characterization producing large volumes of data, manual analysis is no longer practical. To overcome this, we developed a computer vision algorithm, Bok Choy, enabling rapid processing of microscopic images and extracting essential morphological features. In this study, we focus on the automated quantification of crystal size and aspect ratio. However, the computer vision (CV) methods developed here are broadly applicable and can be extended to extract additional crystal features, such as shape descriptors, and spatial distribution, enabling a more comprehensive characterization of crystallization outcomes. Unlike machine learning models, Bok Choy is a rule-based CV framework that does not require training data or supervised learning. Prior to executing

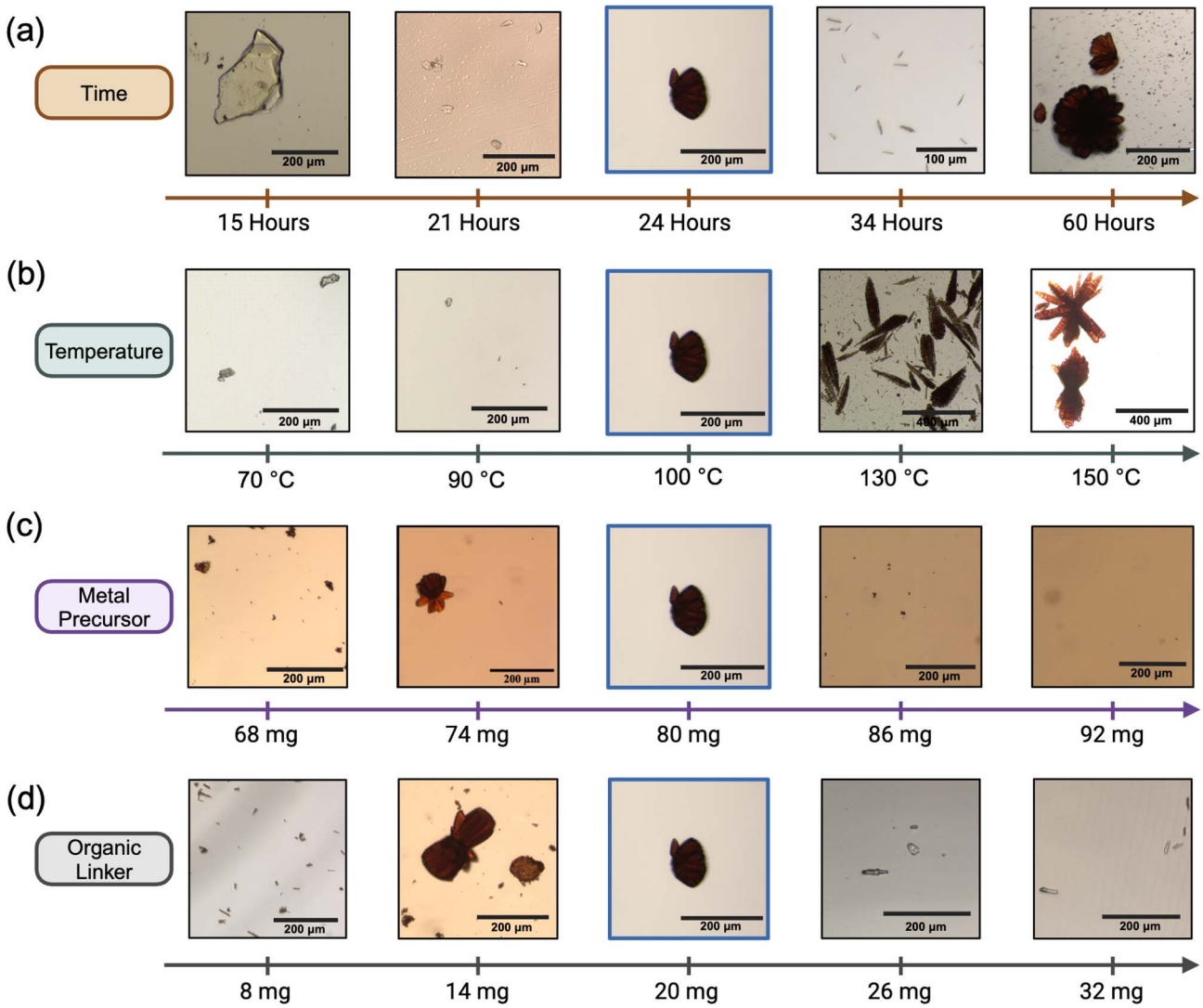

Fig. 3 (a–d) Variation in shape and shape and morphology of the synthesized crystals and different synthesis conditions: (a) time, (b) temperature, (c) metal precursor, and (d) organic linker while keeping the other parameters constant.

the algorithm, human input is required to assess whether microscopic images are suitable for analysis. Once confirmed, the images follow a structured analysis pipeline consisting of preprocessing, contour detection, and classification (see Fig. S3† for an overview of the combined human-Bok Choy workflow). The algorithm follows a structured image analysis pipeline consisting of preprocessing, contour detection, and classification. To address variability and noise in raw microscopy images, a preprocessing step is applied in which each raw image is first converted into binary format. This standardizes lighting and background, enhances crystal contrast, and suppresses background artifacts. Following binarization, contour detection is then applied to identify the boundaries of the detected object, as illustrated in Fig. 4a. The extracted contours are overlaid onto the original microscopic image to ensure consistency in results and enhanced visualization. In the classification step, crystal types are categorized based on shape and size parameters, as shown in Fig. 4b. A convexity index thresholding method was used for all detected contours, where contours with a convexity index higher than 0.865 were classified as isolated crystals or impurities, while those below this threshold were categorized as clusters or overlapping crystals (see Computational methods 5.3).[21] By default, Bok Choy classified objects into isolated crystals and clusters. An optional overlapping crystal detection mode is also available, which further classified contours into isolated crystals, overlapping crystals, and clusters based on morphological deviations (see ESI Section S5.3†). To refine the classification and remove detected impurities, an area-based filtering step is applied. Small detected features below the minimum area threshold are removed, ensuring that only isolated crystals and clusters remain for analysis. The algorithm extracts morphological features, such as aspect ratios and crystal areas, for further data analysis. A representative processed image using the Bok Choy algorithm is shown in Fig. 4c, highlighting the accurate classification of isolated crystals and clusters.

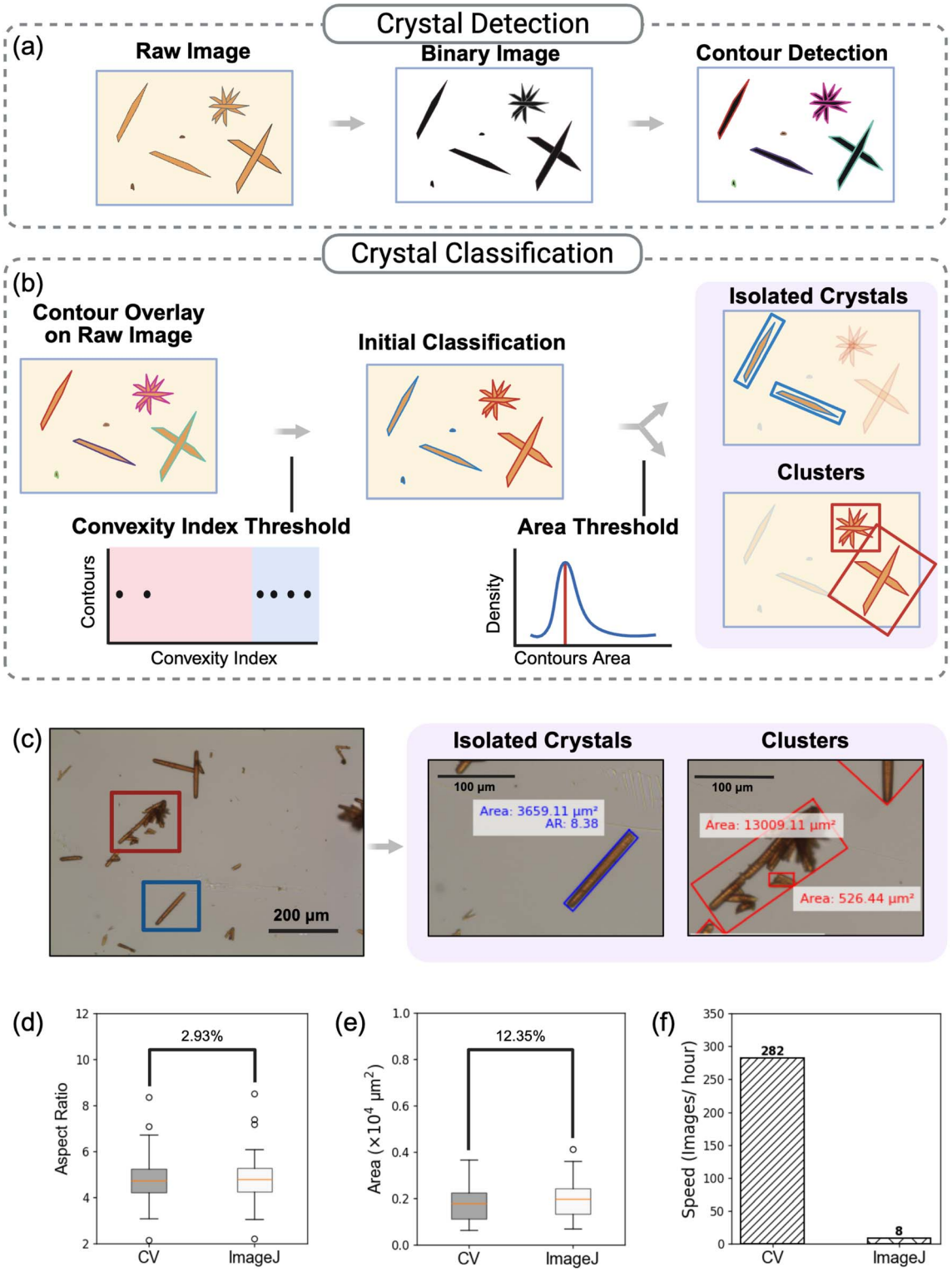

Fig. 4 (a and b) Workflow of the Bok Choy, computer vision algorithm. (a) Image processing workflow for filtering microscopic images. (b) Classification of the detected contours into isolated crystals and clusters using the Bok Choy algorithm. (c) Representative microscopic images of MOF crystals synthesized under SolventVolumes-5I conditions and their corresponding contour classification into isolated crystals and clusters. (d–f) Aspect ratios (d), areas (e), and processing speeds (f) were analyzed using the Bok Choy algorithm and ImageJ software, with relative percentage differences labeled.

A direct comparison of quantifying MOF crystallization outcomes using the Bok Choy Vision Framework and ImageJ, a widely used image processing software, was conducted to validate the accuracy and reliability of Bok Choy. A dataset of 20 isolated crystals from 9 images was selected from Synthesis ID: SolventVolumes-5I and analyzed using both methods. The comparison of aspect ratios, as shown in Fig. 4d, reveals a 2.93% difference between CV and manual crystal detection using ImageJ, indicating a strong agreement in crystal shape analysis. The comparison of crystal area showed an average of 12.35% deviation, reflecting differences in how the two methods define object boundaries during contour detection (Fig. 4e). This deviation arises because ImageJ relies on manual thresholding and segmentation, introducing user-dependent variability and inconsistencies in identifying crystal edges. See ESI Table S2† for additional data on crystal classification for isolated crystals. In contrast, Bok Choy applies an automated, standardized pipeline for contour detection and filtering, leading to more consistent and objective boundary identification. By processing every image using the same preset rules, Bok Choy reduces subjective bias and improves reproducibility. Our results show that Bok Choy demonstrated superior consistency and accuracy in detecting, classifying, and quantifying crystallization outcomes. Moreover, Bok Choy significantly outperformed ImageJ in processing speed. As shown in Fig. 4f, Bok Choy successfully analyzed 282 images per hour, whereas the manual workflow using ImageJ could only process 8 images per hour. This 35-fold increase in efficiency, combined with its automated workflow, established Bok Choy as a robust and scalable tool for rapid and reproducible data processing. The integration of this automated approach enables faster evaluation of synthesis outcomes, facilitating the accelerated synthesis and optimization of MOF materials.

2.5 Solvent engineering for morphological control

Leveraging the computer vision-integrated characterization workflow, the occurrence of crystallization, clustering, or failed crystallization under various solvent compositions was rapidly assessed within each synthesis cycle. The Bok Choy algorithm enabled the correlation of morphological outcomes with the compositions of solvent systems, as shown in Fig. 5a. By keeping temperature, reaction time, and precursor ratios fixed at optimized values determined through synthetic screening in the previous section, we then systematically varied the solvent ratio to study its effect on crystallization behavior. Our solvent engineering investigation revealed distinct regimes: conditions that favored crystal growth, and others that inhibited crystallization, based on three repeated trials. Data from each trial were compared, and the highest-quality images were selected for analysis (see ESI Section S6†). The inset images shown in Fig. 5a represent typical examples for each condition class. Among the three solvents investigated, DMF plays a critical role in Co-MOF-74 formation. Notably, no crystal formation was observed in DMF-free systems from the synthesis conditions in this study, which was attributed not only to its ability to dissolve the H_4dobdc linker, but also to its solvolysis under heating to generate dimethylamine.[20,22] The formation of dimethylamine provided a mild basic environment that facilitated the deprotonation of H_4dobdc to form dobdc^{4-}, enabling coordination with Co^{2+} and initiating nucleation. In contrast, in pure DMF systems lacking solvolytic conditions, dimethylamine generation was suppressed, resulting in insufficient deprotonation and suppressed nucleation. These results highlight the need for binary or ternary solvent systems to achieve controlled crystallization. While further studies are needed to fully understand the complex interactions among solvents, we hypothesize that cosolvents such as water and ethanol serve dual roles in modulating precursor solubility and enhancing the solvolysis of DMF, thereby fine-tuning the crystallization kinetics.[22]

To further investigate solvent-mediated effects on crystal morphology, key morphological features, including aspect ratio and crystal area, were extracted using the Bok Choy algorithm. As shown in Fig. 5b–d, violin plots illustrate the probability distribution of the crystal area or aspect ratios, with red and blue regions marking no crystallization or clustering occurred, respectively. The aspect ratio was analyzed for isolated crystals, while crystal areas were extracted for both isolated crystals and clusters. Priority was given to analyzing isolated crystals before evaluating clusters in the microscopic images.

The results indicated ethanol concentration influenced clustering, as evidenced by the increased presence of cluster-dominated conditions at 40% ethanol (Fig. 5b). Increasing DMF concentration while decreasing water concentration initially led to larger crystals, as reflected in the wider width of the violin plot at 20% before gradually decreasing. This behavior suggested that moderate DMF and water concentration could promote controlled nucleation and growth, while excessive DMF may accelerate deprotonation, leading to excessive nucleation. This caused crystal aggregation and reduced the surface area.[20,23] When DMF concentration was fixed at 20%, a broader range of conditions supported isolated crystal formation, except in high-water-content regions (Fig. 5c). As the water concentration decreased to 20%, the crystal area increased, probably due to an optimized nucleation-growth balance. However, further reducing water concentration below 20% impaired crystallization, suggesting that insufficient water may limit solute transport and coordination interactions, hindering proper crystallization.[24] When water concentration was fixed at 40%, the crystal area remained relatively small, while the aspect ratio exhibited a distinct trend (Fig. 5d). Increasing DMF concentration initially promoted elongated morphologies, but beyond a critical DMF threshold of 40%, the aspect ratio decreased, suggesting that excessive DMF suppressed directional growth, leading to a more isotropic crystal structure. These results underscore the importance of precise solvent composition control in modulating crystal shape and size.

The high-throughput screening approach provides a systematic framework for correlating synthesis conditions with morphological outcomes, accelerating material discovery and the optimization or crystallization protocols. Compared to manual trial-and-error methods, this workflow enables faster condition screening and automated quantitative morphology

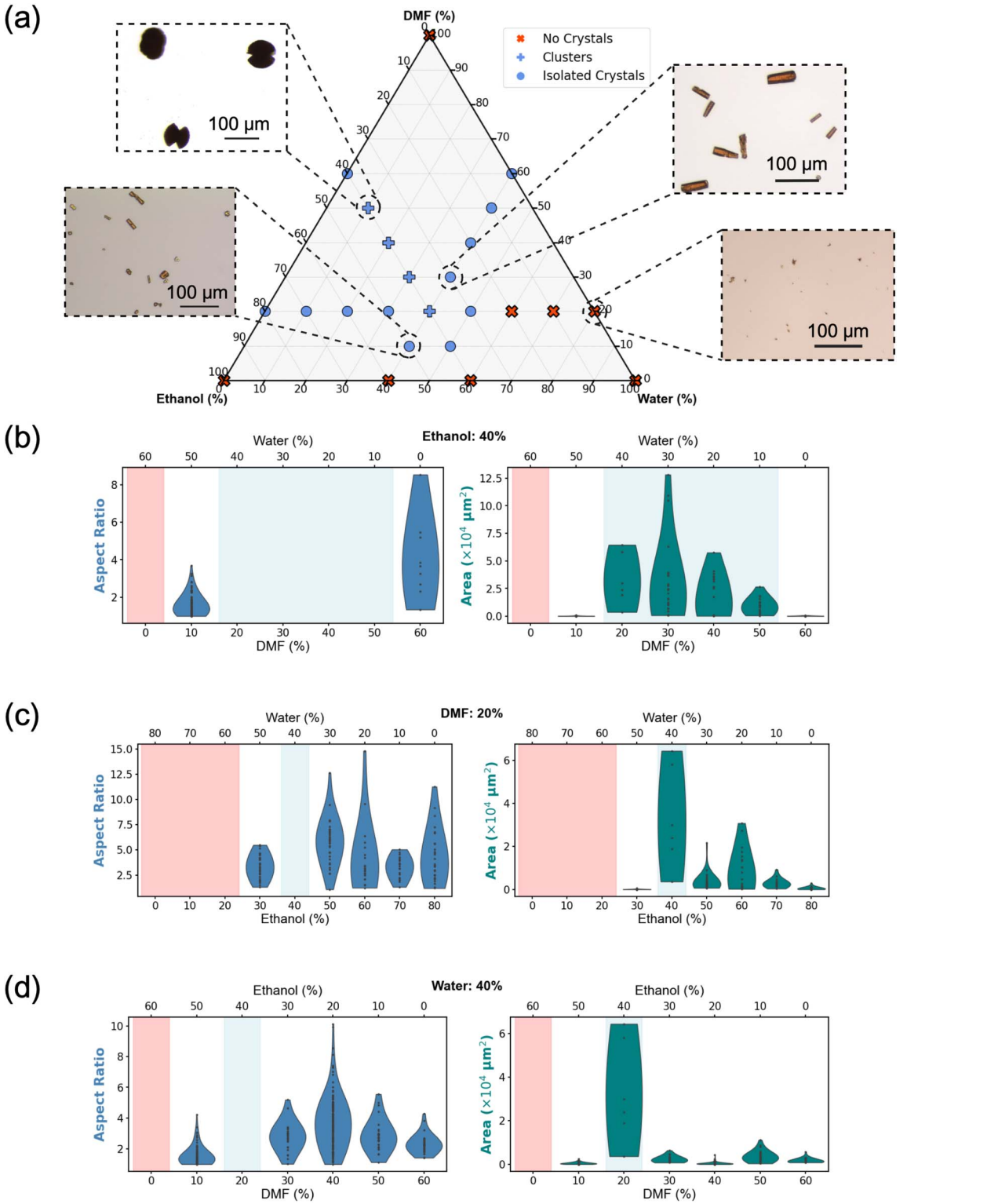

Fig. 5 (a) Ternary plot illustrating the formation of Co_2(dobdc) isolated crystals, clusters, and non-crystalline regions under different solvent conditions. Insets show representative microscopic images of different morphologies. (b–d) Box plots summarizing the aspect ratios and/or areas of the crystals under different solvent conditions: (b) varying the concentrations of DMF and water, while keeping the concentration of ethanol constant at 40%, (c) varying the concentrations of water and ethanol, while keeping the concentration of DMF constant at 20%, and (d) varying the concentrations of DMF and ethanol, while keeping the concentration of water constant at 40%.

analysis. By facilitating a rational strategy for MOF design, it serves as a complementary tool to empirical optimization and contributes to the accelerated synthesis and development of MOF materials.

2.6 Crystallization database construction

With our high-throughput synthesis and characterization efforts, we constructed a new crystallization database for Co_2(dobdc), a representative MOF within the MOF-74 family. In the database, each optical microscopy image is matched with the synthesis conditions, synthesis procedures followed, as well as the metadata of each image stored in a dataset CSV and JSON files. In total, our database contains 787 optical microscopy images tested against 50 unique synthesis conditions. The details of the database are outlined in the ESI.† The database generated in this study has been made publicly available, as listed in the Data availability section, to support future machine learning model development and benchmarking in MOF synthesis.

3 Conclusion

In this study, we successfully developed an integrated experimental and digital workflow that combines high-throughput synthesis with computer vision-based characterization, providing an automated and scalable approach for accelerating materials discovery. By leveraging robot-assisted synthesis using the Opentrons OT-2 liquid handling robot, we improved efficiency, precision, and reproducibility, reducing manual intervention and variability compared to traditional methods.

To further enhance materials characterization, we introduced Bok Choy, a computer vision algorithm that automates the classification of isolated crystals and clusters from microscopic images. Unlike conventional characterization and data processing methods, which often require extensive sample preparation and are time-consuming, this method provides quantitative morphological analysis in a short amount of time, making it a valuable tool for optimizing different synthesis parameters.

Additionally, our workflow facilitated a rapid screening of synthesis parameters to determine the optimal synthesis conditions for MOF crystallization. We observed that the absence of DMF prevents crystallization, while conditions that led to crystallization allowed us to extract morphological information using computer vision. By integrating automation and computer vision, we can efficiently extract crystal morphology data, significantly enhancing the speed, accuracy, and reproducibility of the characterization process.

This workflow has also enabled the creation of large-scale material databases containing microscopic images and extracted morphological features. By systematically compiling crystallization conditions and morphological features, we can expand and structure the database which allows researchers to access, analyze, and build upon the current database, further accelerating machine learning-driven materials discovery. We envision further studies extending this workflow by incorporating machine learning models to predict crystallization outcomes and structure–property relationships from synthesis conditions, enabling autonomous proposal of experimental parameters and fully automated, closed-loop acceleration of MOF discovery.

While the present study focuses on liquid-phase synthesis of Co_2(dobdc), the integrated workflow of automated synthesis and computer vision-based analysis can be adapted to a wide range of synthesis environments, including hydrothermal methods, sol–gel, and potentially solid-state reactions with suitable lab automation. This flexibility highlights the potential of our approach to accelerate materials discovery across diverse materials systems.

Beyond this study, our workflow has broader implications for materials science and chemistry. By integrating automation and high-throughput experimentation, this approach can significantly accelerate the design, synthesis, and optimization of functional materials, reducing reliance on time-consuming trial-and-error methods and facilitating the development of next-generation materials through a systematic, scalable, and reproducible workflow.

4 Experimental methods

4.1 Chemicals

Cobalt(II) nitrate hexahydrate ($Co(NO_3)_2 \cdot 6H_2O$), *N*,*N*-dimethylformamide (DMF), and ethanol (200 proof) were purchased from Fisher Scientific. 2,5-dihydroxyterephthalic acid (H_4dobdc) was purchased from Sigma-Aldrich. All chemicals were used directly without further purification.

4.2 Synthesis of Co_2(dobdc) crystals

The synthesis of Co_2(dobdc) crystals followed a reported method. In a typical process, ($Co(NO_3)_2 \cdot 6H_2O$) (80 mg) and H_4dobdc (20 mg) were dissolved in a mixture of DMF/ethanol/water (10 mL). The resulting solution was heated at 100 °C for 24 h. An Opentrons OT-2 liquid handling robot was used throughout the sample preparation process for solvent transfer and mixing.

4.3 Characterization

Powder X-ray diffraction (PXRD) measurements were taken on a Bruker D8 Discover diffractometer. To prepare MOF samples for PXRD analysis, a portion of the samples was filtered and air-dried to obtain crystalline solids. The dried crystals were subsequently transferred onto the XRD mounting slide. The sample was then gently leveled with a spatula to ensure a flat, evenly distributed powder. In parallel, the samples were allowed to cool to room temperature to minimize post-synthetic changes in crystal morphology, and image acquisition was then performed. The brightfield optical images were captured using an inverted microscope (EVOS FL auto imaging system).

5 Computational methods

5.1 Image preprocessing

Microscopic images with a resolution of 2048 × 1536 were first cropped and converted to grayscale for preprocessing. The scale bar was detected as described in ESI S5.1.† Thresholding was performed using the Mahotas library, which implements Riddler–Calvard's method, due to its ability to automatically determine the optimal threshold value for binarizing the image. Next, the OpenCV library was used to apply morphological closing operations, which smooth the image by removing noise and closing small gaps.

5.2 Contour detection and classification

All contours in the microscopic image were detected using the find_contours() function provided by the Scikit-image library.

5.3 Crystal classification

The convexity index was calculated as:

$$\text{Convexity index} = \frac{\text{contour area}}{\text{convex hull area}} \quad (1)$$

The convexity index threshold was set to be 0.865.[21] Contours with a convexity index greater than this threshold were classified as blue contours, which consist of isolated crystals and impurities. All remaining contours were categorized as clusters and/or overlapping crystals, as illustrated in Fig. S4.†

For all detected blue contours, key parameters such as area and aspect ratio were extracted and visualized in histograms for data analysis. To isolate true isolated crystals from small impurities, a filtering step was performed: contours below the mean area of the blue contour population were removed. The aspect ratios of the filtered isolated crystals (see ESI S5.2†) were then used as a reference distribution for identifying overlapping crystals in subsequent analysis.

Data availability

The code for the Bok Choy computer vision framework is available on the UWSUNLab/CO-MOF GitHub repository (**https://github.com/UWSUNLab/CO-MOF**) with DOI: **https://doi.org/10.5281/zenodo.15116121**. The full microscopic image dataset has been made publicly available on GitHub at uwsunlab/Co-MOF/comof_dataset/images (**https://github.com/uwsunlab/Co-MOF/tree/main/co-mof_dataset/images**) and archived on Zenodo with DOI: **https://doi.org/10.5281/zenodo.15793428**.

Author contributions

Kai Xiang Chong: data curation, formal analysis, methodology, software, visualization, writing – original draft. Qusai A. Alsabia: data curation, formal analysis, investigation, writing – original draft. Zuyang Ye: writing – review & editing. Andrew McDaniel: software. Douglas Baumgardner: resources. Dianne Xiao: resources, supervision. Shijing Sun: supervision, validation, writing – review & editing.

Conflicts of interest

The authors declare no conflicts of interests.

Acknowledgements

The authors gratefully acknowledge Clara Tamura for developing the MOF synthesis Python code for the OT-2 Opentrons liquid handling robot and Tommy Zhang for testing the precision and speed of the liquid handling robot. This research was partially supported by the U.S. National Science Foundation through the UW Molecular Engineering Materials Center (MEM-C), a Materials Research Science and Engineering Center (DMR-2308979 to D. J. X., SEED Award 2024 to S. S.). Generative AI applications, such as ChatGPT, were used to assist in plotting figures and developing the computer vision algorithm, Bok Choy. BioRender (**https://biorender.com**) was used to create illustrations.

References

1 H.-C. Zhou, J. R. Long and O. M. Yaghi, *Chem. Rev.*, 2012, **112**, 673–674.
2 N. Armaroli and V. Balzani, *Energy Environ. Sci.*, 2011, **4**, 3193.
3 X. Liu, S. W. Chee, S. Raj, M. Sawczyk, P. Král and U. Mirsaidov, *Proc. Natl. Acad. Sci. U. S. A.*, 2021, **118**, e2008880118.
4 C. P. Raptopoulou, *Materials*, 2021, **14**, 310.
5 K. A. Colwell, M. N. Jackson, R. M. Torres-Gavosto, S. Jawahery, B. Vlaisavljevich, J. M. Falkowski, B. Smit, S. C. Weston and J. R. Long, *J. Am. Chem. Soc.*, 2021, **143**, 5044–5052.
6 N. Stock and S. Biswas, *Chem. Rev.*, 2012, **112**, 933–969.
7 I. G. Clayson, D. Hewitt, M. Hutereau, T. Pope and B. Slater, *Adv. Mater.*, 2020, **32**, 2002780.
8 Y. Xie, C. Zhang, H. Deng, B. Zheng, J.-W. Su, K. Shutt and J. Lin, *ACS Appl. Mater. Interfaces*, 2021, **13**, 53485–53491.
9 N. L. Rosi, J. Kim, M. Eddaoudi, B. Chen, M. O'Keeffe and O. M. Yaghi, *J. Am. Chem. Soc.*, 2005, **127**, 1504–1518.
10 P. D. C. Dietzel, Y. Morita, R. Blom and H. Fjellvåg, *Angew. Chem., Int. Ed.*, 2005, **44**, 6354–6358.
11 J.-R. Li, R. J. Kuppler and H.-C. Zhou, *Chem. Soc. Rev.*, 2009, **38**, 1477.
12 M. P. Suh, H. J. Park, T. K. Prasad and D.-W. Lim, *Chem. Rev.*, 2012, **112**, 782–835.
13 M. I. Gonzalez, J. A. Mason, E. D. Bloch, S. J. Teat, K. J. Gagnon, G. Y. Morrison, W. L. Queen and J. R. Long, *Chem. Sci.*, 2017, **8**, 4387–4398.
14 *Molecular Profiling: Methods and Protocols*, ed. V. Espina, Springer New York, New York, NY, 2017, vol. 1606.
15 A. Mohammed and A. Abdullah, *Proceedings of 2018 International Conference on Hydraulics and Pneumatics – HERVEX*, Baile Govora, Romania, 2018, pp. 77–85.

16 K. S. Erokhin, E. O. Pentsak, V. R. Sorokin, Y. V. Agaev, R. G. Zaytsev, V. I. Isaeva and V. P. Ananikov, *Phys. Chem. Chem. Phys.*, 2023, **25**, 21640–21648.
17 L. Liu, Z. Chen, J. Wang, D. Zhang, Y. Zhu, S. Ling, K.-W. Huang, Y. Belmabkhout, K. Adil, Y. Zhang, B. Slater, M. Eddaoudi and Y. Han, *Nat. Chem.*, 2019, **11**, 622–628.
18 H. Jiang, Q. Wang, H. Wang, Y. Chen and M. Zhang, *Catal. Commun.*, 2016, **80**, 24–27.
19 W. Lu, E. Zhang, J. Qian, C. Weeraratna, M. N. Jackson, C. Zhu, J. R. Long and M. Ahmed, *Phys. Chem. Chem. Phys.*, 2022, **24**, 26102–26110.
20 J. Łuczak, M. Kroczewska, M. Baluk, J. Sowik, P. Mazierski and A. Zaleska-Medynska, *Adv. Colloid Interface Sci.*, 2023, **314**, 102864.
21 P. Neoptolemou, N. Goyal, A. J. Cruz-Cabeza, A. A. Kiss, D. J. Milne and T. Vetter, *Powder Technol.*, 2022, **399**, 116827.
22 I. Pakamorė and R. S. Forgan, *Digital Discovery*, 2025, **4**(7), 1784–1793.
23 C. Huang, X. Gu, X. Su, Z. Xu, R. Liu and H. Zhu, *J. Solid State Chem.*, 2020, **289**, 121497.
24 B. Zhang, J. Zhang, C. Liu, X. Sang, L. Peng, X. Ma, T. Wu, B. Han and G. Yang, *RSC Adv.*, 2015, **5**, 37691–37696.